12-14-2015

A Multiphysics Modeling of Solid Oxide Metal-Air Redox Battery

Md Ahsan Uddin
University of South Carolina - Columbia

A MULTIPHYSICS MODELING OF SOLID OXIDE METAL-AIR REDOX BATTERY

by

Md Ahsan Uddin

Bachelor of Science
Military Institute of Science and Technology,2010

Submitted in Partial Fulfillment of the Requirements

For the Degree of Master of Science in

Mechanical Engineering

College of Engineering and Computing

University of South Carolina

2015

Accepted by:

Kevin Huang, Director of Thesis

Xinyu Huang, Reader

Lacy Ford, Senior Vice Provost and Dean of Graduate Studies

Acknowledgements

I would like to express my deepest gratitude to my research mentor Dr. Kevin Huang, who gave me the opportunity to pursue my master's degree and suggested my research. I give special thanks to him for his consistent support, guidance, encouragement, patience and teachings. I really appreciate that he took the interest in me and gave me the freedom of learning so that I could face new problems and solve them on my own.

I would like to thank Dr. Meng Guo for his guidance and supervision. I would also like to thank all my previous and current lab colleagues, especially to Dr. Xuan Zhao for her experiment results.

Finally, I would like to thank my parents and my wife for their love and support. Last but not the least I am thankful to God, who constantly guides and protects me from ill fortune.

Abstract

Cost-effective and large scale energy storage is essential for the growth of the future's ''green energy'' infrastructure. Among the energy storage technologies currently being used, rechargeable batteries represent a class of advanced electrical energy storage (EES) mechanisms that can be valuable for the future renewable integration and smart grid. Rechargeable batteries have innumerous advantages over the conventional pumped hydro and compressed-air energy storage system. Now days, There are various types of rechargeable batteries available to work as an energy storage device in a smart grid but it still needs many breakthroughs to become commercially viable for stationary energy storage.

First the development of a new type of battery requires a fundamental understanding of the physical, chemical, mechanical, and electrochemical phenomena involved in the system. By establishing a physics-based mathematical modeling makes it possible to understand the fundamental characteristics and prime criteria of the new battery. My master research project investigates and develops a physics based mathematical model of a novel rechargeable solid oxide metal-air redox battery (SOMARB) which combines a reversible solid oxide fuel cell (RSOFC) and hydrogen-steam chemical looping component. Here hydrogen-steam looping component functions as an "energy storage unit" (ESU) and RSOFC acts as an "electrical functioning unit". One unique feature of this new type of storage battery is the ESU that is physically separated

from RSOFC, allowing the battery to perform fast charging and discharging without concerning the problem arising from volume changes.

The first objective of my master's work is aimed to demonstrate the fundamental electrochemical result and the mass transfer characteristics of the battery through a physics-based mathematical modeling. The second objective of the work is to evaluate the effects of battery's configurational and operational parameters on the performance. The final objective is to establish a more rigorous model to simulate a complete charge and discharge cycle.

In summary, a preliminary theoretical assessment and parametric optimization have been conducted in this study through COMSOL multiphysics modeling tool. Some of the important characteristics of the battery observed in the experiments have been confirmed by the computational results. A number of comparative parametric studies further indicate optimal parameters for a better battery design in the future.

Table of Contents

List of Tables

List of Figures

List of Symbols

E_N	Nernst potential.
SE	Specific energy.
Q	Specific charge.
ΔG	The change of Gibbs Free Energy of the metal-air reaction.
K	Equilibrium constant of the metal-air reaction.
n	Electron number.
F	Faraday's constant.
P	The oxygen partial pressure in air (=0.21atm).
Mo	The atomic weight of oxygen (=16g/mol)
Δm	The mass change of the ESU per area
Kp	The parabolic rate constant of redox kinetics
j	The applied current density
$A_{\partial\Omega_E}$	Area of the RSOFC boundary.
c_i	Molar concentration of gas phase species i

C_{Fe} Total amount of Fe and FeO per unit bulk volume of ESU

$\boldsymbol{d_k}$ Diffusive driving force acting on species k

$D_{i,j}$ Maxwell- Stefan diffusivities

$D_{i,k}$ Multi-component Fick diffusivities

$D_{i,k}^{eff}$ Effective multi-component Fick diffusivities

E Voltage of the battery

$E_{eq,n}$ Equilibrium potential of the anode

$E_{eq,p}$ Equilibrium potential of the cathode

i_{app} Applied current density on the battery

i_n Electrochemical current densities for the anode of RSOFC

i_p Electrochemical current densities for the cathode of RSOFC

$i_{n,o}$ Exchange current density for the anode

$i_{p,0}$ Exchange current density for the cathode

$i_{n,0}^{ref}$ Reference-state exchange current density

j_i Diffusive mass flux vector for species i

k Rate constant for the forward regenerative reaction

k^{-1} Rate constant for the reverse regenerative reaction

M_{Fe} Molar mass of Fe

M_{FeO} Molar mass of FeO

M_k Molar mass for gas phase species k

M_n Mean molar mass of gas mixture

$\mathbf{n}$ Unit normal vector pointing out of the RSOFC boundary

n_{Fe} Amount of Fe

n_{FeO} Amount of FeO

$\boldsymbol{N_i}$ Total mass flux of species i

p Modified pressure

P_A Absolute pressure

P_{ref} Reference pressure

r_i Volumetric molar reaction rate of species

R Universal gas constant

R_i Volumetric mass source of species i

t Time

T Temperature

U	Full-cell Nernst potential of the battery .
V_{ESU}	Bulk volume of ESU
x_k	Mole fraction of species k
α	Anodic transfer coefficient for the anode
β	Anodic transfer coefficient for the cathode
ε_p	Porosity of the ESU
$\varepsilon_{p,0}$	Initial porosity of the ESU
$\emptyset_n$	Solid phase electric potential of the anode
$\emptyset_p$	Solid phase electric potential of the cathode
η	Over voltage of the battery
κ_{br}	Permeability of porous media
μ	Viscosity of gas phase
ρ	Density of domain gas phase
ρ_{Fe}	Density of Fe
ρ_{FeO}	Density of FeO
ω_i	Mass fraction of species i

ξ_{Fe} Conversion for Fe to FeO

ξ_{FeO} Initial conversion for Fe to FeO

∂_{Ω_E} Symbol for the RSOFC boundary

∇ The gradient operator

i Index for gaseous species (i =1for hydrogen and i = 2 for steam)

k Dummy index for species

List of Abbreviations

AFC……..Alkaline Fuel Cell

CAES…….….Compressed Air Energy System

CFD…….Computational Fluid Dynamics

CSE……..Charge Specific Energy

DSE…….……Discharge Specific Energy

EES……...……Electrical Energy Storage

EFU……Electrical Functioning Unit

ESU……Energy Storage Unit

ERB……Electrochemical Rechargeable Batteries

HCL…….Hydrogen Chemical Looping

HESS……..Hydrogen-based Energy storage system

HSFES……High-speed Fly Wheels Energy Storage

ICBs……...Iron/chromium Flow Batteries

IRBs…….Iron Redox Flow Batteries

LABs……..Lead-Acid Batteries

Me/MeO_x……. Metal/Metal oxide

MCFC……Molten Carbonate Fuel Cell

NAS……Sodium Sulfur Battery

Ni-MH……Nickel-Metal Hydride

PHES……Pumped Hydroelectric Energy Storage

PXRD……Powder X-ray Diffraction

RFBs……Redox Flow Batteries

RSOFC……..Regenerative Solid Oxide Fuel Cell

RTE……Round Trip Efficiency

SCES……...Supercapacitors Energy Storage

SMES…….Superconducting Magnetic Energy Storage

SOEC…….……Solid Oxide Electrolytsis Cell

SOFC…….…….Solid Oxide Fuel Cell

SOFeARB……Solid Oxide Fe-air Redox Battery

SOMARB……Solid Oxide Metal-air Redox Battery

SORFB……..……..Solid Oxide Redox Flow Battery

VRBs……..Vanadium Redox Flow Batteries

VBBS……..Vanadium/bromine Flow Batteries

YSZ……Yttria Stabilized ZrO_2

ZBB……..Zinc/bromine Flow Batteries

ZEBRA……...……... "Zeolite Battery Research Africa"

Chapter 1: Overview of the State-of-art Advanced Energy storage Technology

1.1 Introduction

Renewable energy sources, distributed power, and demand response programs can be effectively utilized by a modern electric power grid, which is a requirement of the economy of the twenty-first century. Many technologies that are used in the current electric grid have evolved from the time of Thomas Edison. Thus the electricity industry is in constant need of newer techniques of generating power so that the environmental impact can be reduced, cost reduced and efficiency improved. Methods of cost minimization and improvement of efficiency are areas of focus.

The projected energy needs may be handled by modernizing the electric grid. A sustainable energy delivery system from renewable sources would help in the coming decades to address climate changes. By 2050, the annual electricity requirement of United States would be 4 to 5 tera kilowatt-hours.

The challenges of planning and implementing grid expansion include the balance between economic viability, resiliency, and cyber- security. The impact of carbon emission on environment and the degree of carbon emission are also vital. Energy storage systems (ESS) have the potential to meet these challenges by upgrading the operating

capacity of the grid. It will also aid in mitigating infrastructural investments. ESS can also cater to the special requirements for emergency situations. Issues with timing, transmission, and dispatch of electricity can also be addressed by ESS. At the same time the quality and reliability of the power generated by traditional and variable sources of power can also be addressed. Modernizing the grid will require a substantial deployment of energy storage. In the past few years, the urgency of energy storage requirements has become a greater, more pressing issue that is expected to continue growing over the next decade.

Renewables are the fastest growing resources being developed among all the types of energy production. This is primarily due to its natural abundance, wide accessibility and environmental friendliness. The annual rate of electricity generation is 3.1% and the renewable share in the world's electricity generation is projected to increase from 19% in 2008 to 23% by 2035. The technology of EES is a key to harnessing energy from renewable resources efficiently and reliably, which lies in the availability of a technology that is capable of leveling off the intermittency presented by renewable energy resources to electric grid.

The balance between energy supply and demand can be maintained by EES device. It stores electricity when it is in excess for the later use. It plays an important role to ensure grid reliability and grid stability.

1.2 EES performance parameter

Rechargeable batteries are an important class of EES technology. To evaluate the performance of a battery, some necessary parameters have to be considered.

- Battery State of Charge (BSOC)

A key parameter of a battery in use is the battery state of charge (BSOC). The BSOC is defined as the fraction of the total energy or battery capacity that has been used over the total available from the battery.

- Depth of Discharge

In many types of batteries, the full energy stored in the battery cannot be withdrawn (in other words, the battery cannot be fully discharged) without causing serious, and often irreparable damage to the battery. The Depth of Discharge (DOD) of a battery determines the fraction of power that can be withdrawn from the battery. For example, if the DOD of a battery is given by the manufacturer as 25%, then only 25% of the battery capacity can be used by the load.

- Charging and Discharging Rates

The charging rate, in Amps, is given in the amount of charge added the battery per unit time (i.e., Coulombs/sec, which is the unit of Amps). The charging/discharge rate maybe specified directly by giving the current - for example, a battery may be charged/discharged at 10 A. However, it is more common to specify the charging/discharging rate by determining the amount of time it takes to fully discharge the battery.

- Charging and Discharging Regimes

Each battery type has a particular set of restraints and conditions related to its charging and discharging regime, and many types of batteries require specific charging regimes or charge controllers. For example, nickel cadmium batteries should be nearly completely discharged before charging, while lead acid batteries should never be fully discharged. Furthermore, the voltage and current during the charge cycle will be different for each type of battery. Typically, a battery charger or charge controller designed for one type of battery cannot be used with another type.

- Battery Capacity

"Battery capacity" is a measure (typically in Amp-hr) of the charge stored by the battery, and is determined by the mass of active material contained in the battery. The battery capacity represents the maximum amount of energy that can be extracted from the battery under certain specified conditions. However, the actual energy storage capabilities of the battery can vary significantly from the "nominal" rated capacity, as the battery capacity depends strongly on the age and past history of the battery, the charging or discharging regimes of the battery and the temperature.

- Impact of Charging and Discharging Rate

The charging/discharging rate affects the rated battery capacity. If the battery is being discharged very quickly (i.e., the discharge current is high), then the amount of energy that can be extracted from the battery is reduced and the battery capacity is lower. This is due to the fact the necessary components for the reaction to occur do not necessarily have enough time to either move to their necessary positions. Only a fraction of the total reactants are converted to other forms, and therefore the energy available is reduced. Alternately, the battery is discharged at a very slow rate using a low current, more energy can be extracted from the battery and the battery capacity is higher.

- Temperature dependence

The temperature of a battery will also affect the energy that can be extracted from it. At higher temperatures, the battery capacity is typically higher than at lower temperatures.

- Voltage Efficiency

The voltage efficiency is determined largely be the voltage difference between the charging voltage and voltage of the battery during discharging. The dependence of the battery voltage on BSOC will therefore impact voltage efficiency. With other factors being equal, a battery in which the voltage varies linearly with BSOC will have a lower efficiency than one in which the voltage is essentially constant with BSOC.

- Energy Density

The amount of energy stored in a given system per unit volume (KWh/L) or (MJ/L).

- Power Density

The power density of a battery is related to its energy density, as well as the ability of the battery to discharge quickly.

- Self-Discharge

Self-discharge refers to the fact that even in the absence of a connected load, the discharge reaction will proceed to a limited extent and the battery will therefore discharge itself over time. The rate of self-discharge depends primarily on the materials involved in the chemical reaction

- Battery Lifetime

Since batteries inherently involve chemical reactions that are reactive, the materials used in batteries are susceptible to alternate reactions that degrade battery performance. While certain catastrophic battery failure mechanisms are possible, battery lifetime is typically controlled by the gradual degradation in battery capacity which accompanies charge/discharge cycles.

- Cost of energy storage: The cost per unit stored in unit of $/KWh.
- Safety: Safe operation over a meaning fully long period of time.

1.3 The state of the art EES technologies

A widely-used approach for classifying EES systems is the determination according to the form of energy used. In Figure 2-1 EES systems are classified into mechanical, electrochemical, chemical, electrical and thermal energy storage systems.

Mechanical energy storage systems are three types:

- Pumped hydro – PHS
- Compressed air – CAES
- Flywheel – FES

Electrochemical energy storage systems are two types:

- Secondary batteries (Lead acid / NiCd / NiMh / Li / NaS)
- Flow batteries (Redox flow / Hybrid flow)

Chemical Energy storage systems:

- Hydrogen (Electrolyser / Fuel cell / SNG)

Electrical energy storage systems:

- Double layer capacitor- DLC
- Superconducting magnetic coil – SMES

Thermal energy storage systems:

- Sensible heat storage (Molten salt / A-CAES)

1.3.1 Pumped hydro energy storage– PHS

Pumped hydro energy storage systems are by far the largest storage technology available. It represents nearly 99% of worldwide installed electrical storage capacity which is about 3% of global generation capacity with over 120GW pumped hydro storage power plants. Hydro storage systems use two water reservoirs at different elevations to pump water

during off peak hours from the lower to the upper reservoir (charging). The water flows back from the upper to the lower reservoir, powering a turbine with a generator to produce electricity (discharging) when required. There are different options for the upper and lower reservoirs, e.g. high dams can be used as pumped hydro storage plants. A typical facility has 300m of hydraulic head, and the energy storage capacity is a function of the reservoir volume and hydraulic head.

1.3.2 Compressed air energy storage:

Compressed air (compressed gas) energy storage is a technology known and used since the 19th century for different Industrial applications including mobile ones. Air is used as storage medium due to its availability. Electricity is used to compress air and store it in either an underground structure or an above-ground system of vessels or pipes. When needed the compressed air is mixed with natural gas, burned and expanded in a modified gas turbine. Like PHS, CAES can be manufactured and assembled at a very large scale. Typical power capacities for a CAES system range from 50 to 300MW.

1.3.3 Flywheel energy storage (FES):

In flywheel energy storage (fig 1.1) rotational energy is stored in an accelerated rotor, a massive rotating cylinder. The main components of a flywheel are the rotating body/cylinder (comprised of a rim attached to a shaft) in a compartment, the bearings and the transmission device. The energy is maintained in the flywheel by keeping the rotating body at a constant speed. An increase in the speed results in a higher amount of energy stored. In general, flywheels cost more than batteries in initial investment, despite requiring less maintenance.

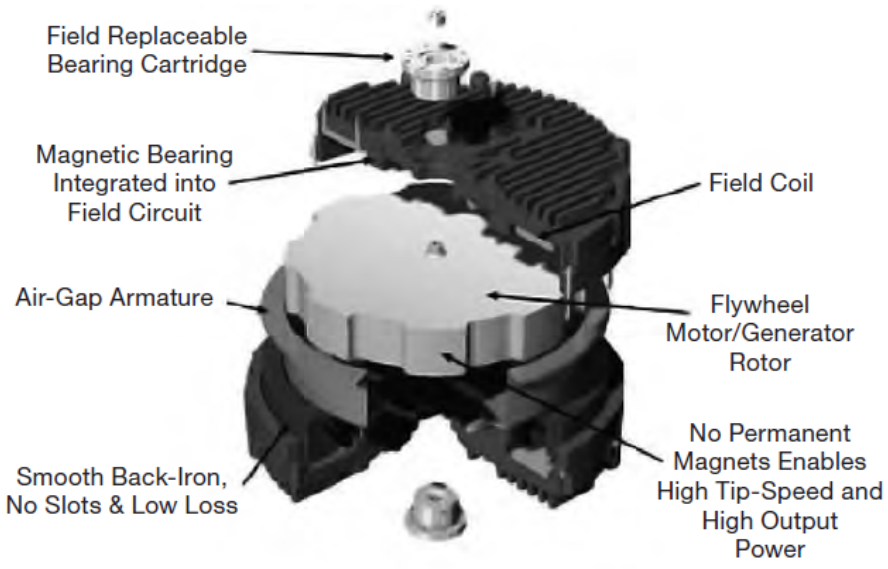

Figure 1.1 : Flywheel energy storage

1.3.4 Double-layer capacitors (DLC)

Electrochemical double-layer capacitors (DLC), also known as super capacitors, have been known for 60 years. This is a relative recent technology in the field of short term energy storage system. In a double layer capacitor for one or both electrodes, consist of a porous structure of activated carbon which is immersed into an electrolytic solution (typically potassium hydroxide or sulphuric acid). A separator is used to restrict the physical contact of the electrodes but allows ion transfer between them. As shown in the schematic view of its internal components of fig. 1.2, between each electrode and the electrolyte, this structure effectively creates two equivalent capacitors connected in series. At the interface between the solid electrode material and the liquid electrolyte in the micropores of the electrodes, energy is stored as a charge separation in the double layer formed.

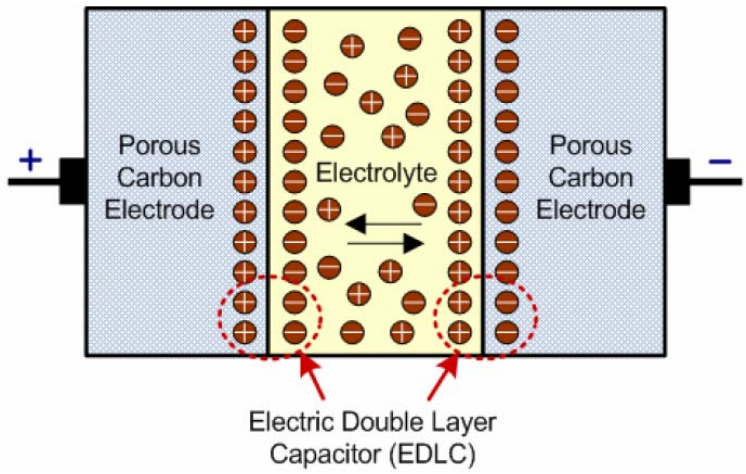

Figure 1.2 : Schematic view of a Double Layer Capacitor

They fill the gap between general batteries and classical capacitors used in electronics. Their nearly unlimited cycle stability as well as extremely high power capability and their many orders of magnitude higher energy storage capability, when compare to traditional capacitors. Super capacitors are also one type of electrochemical cells inside microstructure of electrodes, without any redox reactions taking place at the electrodes. Super capacitors can be connected in series or in parallel. It has energy densities of 20MJ/m^3 to 70 MJ/m^3 with a cycle efficiency of 95%. The main shortcomings of such kind of EES system is self-discharge, which is around 5% per day. [1, 2]

1.3.5 Thermal storage systems:

Thermal (energy) storage systems store available heat by different means in an insulated repository for later use. Solar panel used to focus the suns energy which heats up a low melting point salt until becomes liquid and to generate steam which in turns drives a turbine to generate electricity. Another use of this thermal energy storage system is to make ice from water or some another way to absorb energy and later on by using this energy to cool

building. Since the major part of the thermal energy storage comes from the sun but as the sun is not consistent all over the year, so it cannot be a solution of a reliable energy storage system.

1.3.6 Hydrogen based energy storage systems:

A hydrogen storage system comes with a storage tank, an electrolyzer and a fuel cell. Water splits into hydrogen and oxygen with the help of electricity by an electrochemical converter. For an open-ended time space, hydrogen can be concentrated in gas reservoirs. Electricity is generated as hydrogen and oxygen combine and react together in the fuel cell under an electrochemical reaction by releasing heat. Because of cost effectiveness, oxygen is then withdrawn out to the air from the reservoirs and eventually collected to generate power.

1.3.7 Redox flow battery:

"Redox" comes from the chemical reaction reduction and oxidation reaction employed in the RFB to store energy. Liquid electrolyte solutions containing dissolved metal ions as active masses which flow through a battery of electrochemical cells during charging and discharging in a redox flow battery. Current RFBs can be classified according to the anolyte and catholyte chemistries into: iron/chromium flow batteries (ICBs), polysulphide/bromine flow batteries (PSBs), all vanadium redox flow batteries (VRBs), vanadium/bromine flow batteries (VBBs), zinc/bromine flow batteries (ZBB), vanadium/cerium flow batteries, soluble lead-acid batteries (e.g. lead-carbon batteries), all iron redox flow batteries (IRBs), etc. [3],[4]

1.3.7 Lead acid battery:

Lead acid batteries are the world's most widely used batteries that have been commercially deployed since about 1890. In the past, many lead acid batteries were used for storage in grids. Stationary lead acid batteries have to meet far higher product quality standards than starter batteries. Typical service life is 6 to 15 years with a cycle life of 1 500 cycles at 80 % depth of discharge, and they achieve cycle efficiency levels of around 80 % to 90 %. In 1988 , a 10 MW/40 MWh flooded lead acid system was installed at the chino substation of Southern California Edison Company for load leveling.[5] . The major limitation of lead acid battery is high maintenance cost since it is highly sensitive to the environment. The typical temperature for a lead acid battery is 27◦C.

1.3.8 Nickel cadmium and nickel metal hydride battery

Before the commercial introduction of nickel metal hydride (NiMH) batteries around 1995, nickel cadmium (NiCd) batteries had been in commercial use since about 1915. Compared to lead acid batteries, nickel-based batteries have a higher power density, a slightly greater energy density and the number of cycles is higher. However, the nickel electrode still suffers from low energy density, high self-discharge rate (e.g., 2% to 5% loss per month) and the 'memory effect' of incomplete discharge prior to a new recharge. Its lifespan is around 500-1000 cycles, with a broad variation on how the batteries are used. Another problem is the poor scalability.

1.3.9 Lithium ion battery (Li-ion):

Lithium ion batteries have become the most important storage technology in the areas of portable and mobile applications. One lithium ion cell can replace three NiCd or NiMH cells which have a cell voltage of only 1.2 Volts. Safety is a serious issue in lithium ion battery technology. It has a slow self-discharge and less than half that of nickel based batteries. This type of battery doesn't need periodic discharge. It can also provide higher densities without any periodic discharge. It also has some limitation. This type of battery is subject to aging and is also expensive to manufacture.

1.3.10 Sodium sulfur battery (NaS):

Sodium sulfur batteries consist of liquid (molten) sulfur at the positive electrode and liquid (molten) sodium at the negative electrode and active materials are separated by a solid beta alumina ceramic electrolyte. It is by far best suited for large-scale stationary applications. The temperature of the battery is kept between 300 °C and 350 °C to keep the molten electrodes in the same state. It can meet the short term as well as long term discharge applications. The key advantages of NAS batteries include high energy density, high rate capacity, negligible self-discharge, high RTE (~85%), high cycle life and good sustainability. It can meet either the short-term or long-term discharge applications. The flexibility makes it superior over many other batteries for energy management and power quality applications. However, the electrode materials have a very high reactivity in liquid state, so the safety issue is of a great concern. Another drawback of this battery is its inability to thermal cycling.

1.3.11 Sodium nickel chloride battery (NaNiCl):

The sodium nickel chloride (NaNiCl) battery is also known as the ZEBRA (Zero Emission Battery Research) battery. It is also a high temperature battery like the NaS battery. The working temperature of ZEBRA ranges from 270 to 350℃, and the OCV is around 2.61V per cell. The theoretical specific energy density of individual cell is 790 Wh/kg, which is slightly greater than that of NAS cells, 760 Wh/kg [6] Safety tests in Switzerland showed that these batteries are much safer than NAS cells, and do not represent a significant risk under simulated crash conditions during transportation application [7]

1.3.12 Metal air batteries:

A metal air electrochemical cell consists with anode as a pure metal and cathode connected to an inexhaustible supply of air. Only the oxygen in the air is used for the electrochemical reaction. The development of metal-air batteries experienced a halt due to material problems at air electrode, thermal management, and etc.[8] . Recent advances in the performance and stability of air cathodes [50, 51] and improved anode materials [9-11] along with their extremely high energy density nature have spurred a great interest to revisit this old technology for energy storage.

Metal air batteries are two types based on electrolytes one is aqueous electrolyte and the other is based on a water sensitive aprotic solvents. Al-air, Fe-air and Zn-air batteries use aqueous electrolytes. The generic battery reactions for M-air (M=Al or Fe) are

$$Anode:\ Me + xOH^- \underset{Charge}{\overset{Discharge}{\rightleftharpoons}} Me(OH)_x + xe^-$$

$$Cathode: O_2 + 2H_2O + 4e^- \underset{Charge}{\overset{Discharge}{\rightleftharpoons}} 4OH^-$$

$$Overall: Me + \frac{x}{4}O_2 + \frac{x}{2}H_2O \underset{Charge}{\overset{Discharge}{\rightleftharpoons}} Me(OH)_x$$

Lithium air batteries are typically based on Li^+ -ion conductors but due to its poor recharge ability [12, 13] and inferior energy output as well as high cost is being seriously challenged as a commercial product. Although refueling unit for zinc air battery has been offered by many manufacturers, where the consumed metal is mechanically replaced and processed separately. Rechargeable metal-air batteries that are under developed have a lifetime of only a few hundred cycles (for Zn-air) and the efficiency is below 50% [10]. All these issues call for discovery of new materials and innovative design for metal-air batteries.

1.4 Summary

During the Northwest blackout of 2003 Ohio, Michigan, Canada and New York City went under darkness. It started from Ohio then that brought darkness to the New York City named "the city never sleeps". Nobody sabotaged the grid, neither was there an earthquake. The US electricity grid was same. It came out later that there was a computer failure at that time. According to Imre Gyuk, who manages the Energy Storage Research Program at the U.S. Department of Energy, "we can avoid massive blackouts like the big one in 2003 by

storing energy on the electric grid. Energy could be stored in units at power stations, along transmission lines, at substations, and in locations near customers". Grid energy storage can be used to store electricity on a large scale within an electrical power grid. When production exceeds consumption electrical energy is stored and this energy is used when consumption exceeds production. The principal requirements for a grid-scale energy storage system include fast response, high energy storage capacity, high power capacity, high rate capacity, high round-trip efficiency, long cycle life, safety, sustainability and scalability, all of which have a great impact on the final product cost.

PHES and CAES have a limitation on geography in many ways rather than electrochemical energy storage systems which are more flexible to integrate into a smart grid. Many of the batteries have been proposed now days but in total they are less than 1% in total.[6]

Redox flow batteries, NAS, NaNiCl stand out the efficient technology so far for grid energy storage. Though redox flow battery is important for grid energy storage due to its simple design but for high energy densities and fast and deep discharge/charge cycling capability NAS/ZEBRA have come out as a frontier of grid energy storage. Unsustainable thermal cycling, high manufacturing cost as well as unsafe nature are the shortcomings for NAS/ZEBRA. Inexhaustible cathode reactants, potential cost reduction and extremely high energy density metal air batteries have come into focus for grid energy storage now days. However, in materials development and system design, metal air batteries are facing many challenges. To overcome this hurdle new battery chemistry and innovative design is necessary to commercialize the high-potential metal air rechargeable batteries. Recently, a distinct group of solid oxide redox flow batteries targeted at stationary energy storage was developed based on the technologies of reversible solid oxide fuel cell (RSOFC) and H_2

chemical looping[14-21]. My master's research is aimed to simulate all the characteristics of this type of battery with an improved design. In the following subchapters, characteristic simulations of this novel Solid Oxide Metal air battery (SOMARB) system based on solid oxide fuel cell (SOFC) and Hydrogen Chemical Looping (HCL) technologies is explained as a new EES mechanism suitable for stationary storage.

Chapter 2: Theoretical aspects of analytic modeling

As early as 170 years ago fuel cell became known in scientific world and the first SOFC was demonstrated more than one century later in 1940s [22, 23]. However, it was not until 1980s that the first reversible SOFC (RSOFC) was operated as both power and hydrogen generators [24]. It can reversibly convert the chemical energy in hydrocarbon fuels to electrical energy and split water and CO_2 into H_2 and CO with DC electrical energy input with high conversion efficiency. By using these characteristics of a reversible solid oxide fuel cell (RSOFC) a unique battery has been developed where RSOFC can be reversibly converted into chemical energy by a physically separated metal-metal oxide (Me-MeOx) redox couple. This physically separated redox couple leads the battery to high efficiency and easy system integration without impacting the battery's structural integrity.

Experimental studies of this novel battery are currently being carried out in our group but understanding the complex physical, chemical, mechanical, and electrochemical phenomena involved in the system, would greatly benefit the development of the battery. A mathematical modeling based on physics would be an ideal tool to meet this demand. So far very little modeling work on this type of battery has been reported. In 2012, Ohmoti et al [25] proposed a simplest configuration to study the battery characteristics

and later on in 2013 Meng Guo [26] developed a multi-physics model based on a 2D axial symmetric geometry. But there are some limitations in both the models. At first Ohmoti considered only 1D Fick's diffusion model with the simplest configuration to study the battery's characteristics; but to understand the battery characteristics properly much more rigorous multi-physics model is required. Later on the transport phenomena in the concentrated gas phase has been demonstrated being solved through a simple way by Guo, but no charging profile was studied. So the major objective of this work is to develop a more rigorous multi-physics model than the Ohmoti's 1D model, which would encompass most of the transport and kinetic processes involved in the solid oxide redox flow batteries and simulate both charge and discharge profiles.

2.1 Early concept of SOMARB

To develop energy storage system Metal/Metal oxide redox couple with the combination of a RSOFC was first proposed in 1996 in a patent filed by two Westinghouse engineers Dr. Arnold Isenberg and Dr. Roswell Ruka. Fe/FeO redox-couple bed integrated with bundles of cathode-supported RSOFCs in their patent. During the fuel-cell discharge mode H_2O is led to oxidize Fe to produce H_2 in the redox couple bed. On the other hand during the charging mode H_2 is electrically split from H_2O which is then utilized to reduce FeO back to Fe. This concept is the foundation of our novel "solid oxide metal air redox battery" technology which is built upon the substrate of an anode instead of cathode.

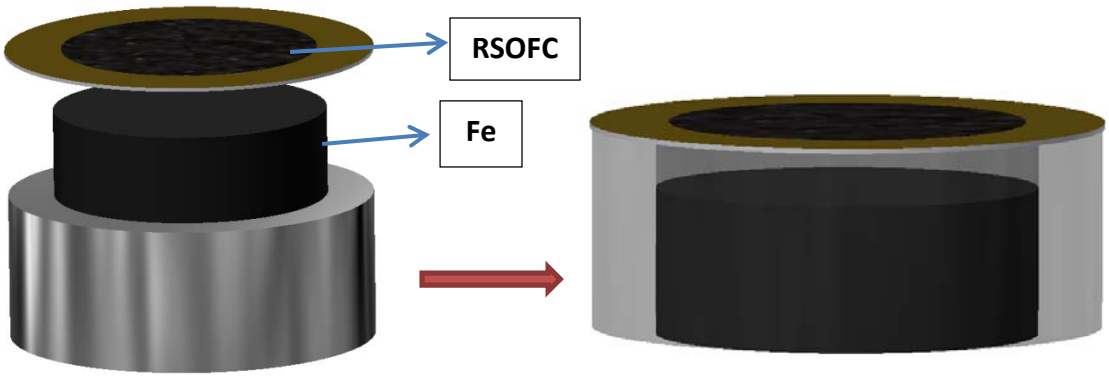

Figure 2.1 : Assembled figure of SOMARB

2.2 Working principles of advanced SOMARB

The multiphysics model is presented here is developed for a closed loop cylindrical battery reactor working at 800℃ . According to figure 2.1 this battery system includes a cylindrical reactor that carries out the battery's functionality. The cylindrical reactor can be regarded as the combination of a RSOFC and a redox cycle unit (RCU). The RSOFC has a planer disk and is sealed at the top of the cylindrical reactor facing the interior space of the cylindrical reactor. A packed bed containing porous Fe based redox couple pellets RCU is right below the RSOFC.

The new battery is based on hydrogen chemical looping technology and an anode supported tubular RSOFC. Here RSOFC acts as an electrical functioning unit and a metal/metal oxide (Me/MeOx) redox couple as the energy storage unit (ESU). Atmosphere containing inexhaustible cathode reactant – air is available towards air electrode of RSOFC and a closed loop is created to ensure energy transfer through electrochemical reaction and chemical equilibrium among H_2-H_2O-Me-MeOx in the fuel electrode.

During the discharge cycle, Me is oxidized by H_2O to form MeOx and H_2; the latter is then electrochemically oxidized into H_2O by RSOFC operating as a fuel cell, and the formed H_2O continues to react with Me to produce more H_2 to sustain the discharge cycle. When all Me (or a controlled portion) is oxidized, the discharge cycle is stopped, and the battery needs to be recharged. During the charge cycle, RSOFC operates as an electrolyzer with electricity as energy input to split H_2O into H_2; the latter then reduces MeOx into Me in the ESU, and the formed H_2O continues to be electrochemically split into H_2 to sustain the charge cycle. When all MeOx (or a controlled portion) is reduced, the battery is ready for the next-round discharge cycle. In accordance with Gibb's Phase Rule, the gas composition, i. e., the ratio of partial pressures of H_2 to H_2O, of the oxygen shuttle H_2-H_2O remains constant during the battery's cycles, resulting in a state-of-charge independent Nernst potential, while only the mass ratio between Me and MeOx varies with the state-of-charge. The overall chemical reactions following the electrical cycles are illustrated in the right side of Fig.2.2.

During the charge and discharge cycles, the oxygen evolution and reduction occur at the air-electrode, respectively, which leads to the following global battery reaction:

$$Me + \frac{x}{2} O_2 \underset{charge}{\overset{discharge}{\rightleftarrows}} MeOx \tag{1}$$

This reaction essentially suggests a "metal-air" chemistry nature of the SOMARB.

The reaction loop in the ESU during the charge and discharge cycle is as follows:

$$H_2O + Fe \underset{charge}{\overset{discharge}{\rightleftarrows}} H_2 + FeO$$

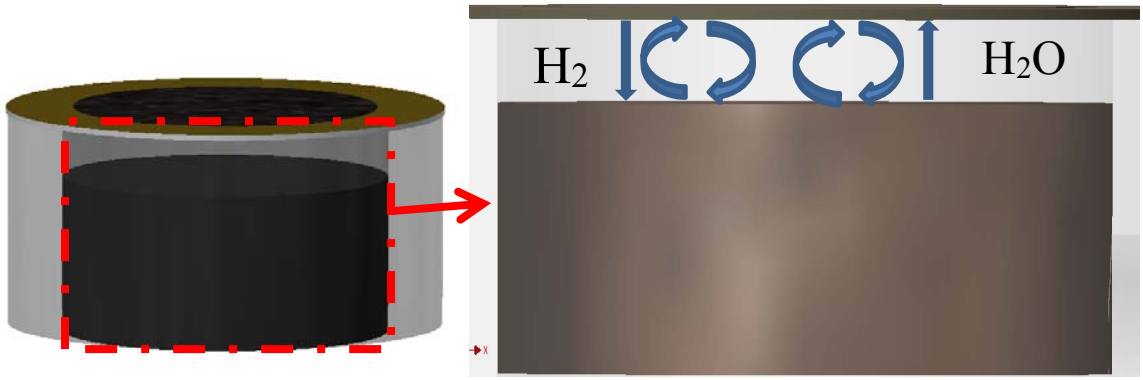

Figure 2.2 : Working principle of SOMARB

2.3 The mass transports in the RCU domain and free-flow phase

The Maxwell–Stefan diffusion (or Stefan–Maxwell diffusion) is a model for describing diffusion in multicomponent systems. The equations that describe these transport processes have been developed independently and in parallel by James Clerk Maxwell for dilute gases and Josef Stefan for fluids. In the free-flow phase, between RSOFC and a packed-bed containing porous Fe-based redox couple pallets, the multi-component mass transfer for concentrated species is governed by the Maxwell-Stefan diffusion and convection. The governing equation for Maxwell Stefan diffusion equation:

$$\frac{\partial \omega_i}{\partial t}\rho + \nabla . \underline{j_i} = R_i \quad (i = 1,2) \quad \text{.....(1)}$$

Where ω_i is the mass fraction of species i, ρ is the density of gas phase, $\underline{j_i}$ is the diffusive mass flux vector for species i and R_i is the volumetric mass source of species i , Here

subscript $i = 1$ stands for hydrogen and $i = 2$ stands for steam. The expression for diffusive mass flux vector, j_i

$$j_i = -\rho\omega_i \sum_k \breve{D}_{i,k}^{eff} \underline{d}_k \quad \text{.....(2)}$$

Where $\breve{D}_{i,k}$are the multi-component Fick's diffusivities, $\underline{d}_k$(in the unit of 1/m) is the diffusive driving force acting on species k, and subscript k is a dummy index for species. According to ref. [27], the values of $\breve{D}_{i,k}$ can be calculated from the multi-component Maxwell- Stefan diffusivities, $\breve{D}_{i,j}$ (where $i \neq j$ and $\breve{D}_{i,j} = \breve{D}_{j,i}$); therefore for this binary system, only the value of $\breve{D}_{i,k}$ is needed to implement the model. In this work, the hydrogen/steam mixture is regarded as ideal gas and the diffusive driving forces are expressed as:

$$\breve{D}_{i,k}^{eff} = D_{i,k}\varepsilon_P^{3/2} \quad \text{.....(3)}$$

$$\underline{d}_k = \nabla x_k + \frac{1}{P_A}[(x_k - \omega_k)\nabla P_A] \quad \text{.....(4)}$$

Where $\varepsilon_P$the porosity of RCU is x_k is the mole fraction of species k and $P_A$is the absolute pressure. The mole fraction x_k can be calculated as:

$$x_k = \frac{\omega_k}{M_k} M_n \quad \text{.....(5)}$$

$$M_n = (\sum_k \frac{\omega_k}{M_k})^{-1} \quad \text{.....(6)}$$

Where $M_k$the molar is mass for species k and M_n is the mean Molar mass for the gas mixture. Now if we look into the equation:

$$H_2O + Fe \underset{Charge}{\overset{Discharge}{\rightleftharpoons}} H_2 + FeO$$

Here for the discharge, amount of steam reacts with Fe turns to FeO and H_2 and during charge, amount of H_2 reacts with FeO turns to Fe and steam, is fully depends on concentration of reactants in both the gas phase (hydrogen and steam) and the solid phase (Fe and FeO). Let ξ_{Fe} represents the conversion of Fe to FeO. So from that it can easily say that the molar fractions of Fe and FeO are respectively proportional to $1 - \xi_{Fe}$ and ξ_{Fe}. By assuming the reaction orders equal the stoichiometric coefficients the volumetric molar reaction rate for hydrogen and steam, r_1 and r_2 , can be expressed as according to[26]:

$$r_1 = k(1 - \xi_{Fe})c_2 - k^{-1}\xi_{Fe}\, C_1 \quad \text{.....(7)}$$

$$r_2 = -r_1 \text{.....(8)}$$

Here $C_1$and C_2 are the molar concentrations of hydrogen and steam, and k and k^{-1}(in units of 1/s) are respectively the rate constants for the forward and reverse reactions. The volumetric mass source terms R_i, where i represent for species i and M_i represents the molar reaction rate.

$$R_i = r_i M_i \quad (i=1, 2) \text{.....(9)}$$

According to the ideal gas law we can find out the molar reaction rate for species i

$$C_i = \frac{x_i P_A}{RT} \text{.....(10)}$$

Here T represents the temperature (K) and R is the universal gas constant. Now the governing equation for the mass balance relates with the reaction rate is as follows:

$$C_{Fe}\frac{\partial \xi_{Fe}}{\partial t} = r_1 \quad \text{.....(11)}$$

Here C_{Fe} represents the total amount of Fe and FeO per unit bulk volume of RCU. So C_{Fe} can also be written as:

$$C_{Fe} = \frac{n_{Fe}+n_{FeO}}{V_{RCU}} \quad \text{.....(12)}$$

Here n_{Fe} and n_{FeO} (in the unit of mole) represents the amounts of Fe and FeO, and V_{RCU} is the bulk volume of RCU. Since for 800℃ the conversion between Fe and FeO is equal molar so the value for $n_{Fe} + n_{FeO}$ remains constant and is equal to the total number of Fe and FeO in the initial RCU loading. As Fe and FeO have different molar volume values, the porosity ε_P may change with the progress of reaction and now the correlation between ε_P and ξ_{Fe} is derived as follows according to[26]

$$\varepsilon_P = \varepsilon_{P,0} + C_{Fe}\left(\frac{M_{Fe}}{\rho_{Fe}} - \frac{M_{FeO}}{\rho_{FeO}}\right)(\xi_{Fe} - \xi_{Fe,O}) \quad \text{.....(13)}$$

Here $\varepsilon_{P,0}$ is the initial porosity of RCU, ξ_{FeO} is the initial conversion of Fe to FeO, M_{Fe} and M_{FeO} are the molar masses of Fe and FeO, respectively.

2.4 The electrochemical sub-model at the RSOFC boundary

The mass flux at the RSOFC boundary of the gas phase species are coupled to the electrochemical current density, i_n:

$$-\underline{n}.\underline{J}_1 = -\frac{i_n M_1}{2F} \quad \text{.....(14)}$$

$$-\underline{n}.\underline{J}_2 = \frac{i_n M_2}{2F} \quad \text{.....(15)}$$

Here $\underline{n}$ is the unit normal vector pointing out of the RSOFC boundary, i_n is the anode current density of the RSOFC, and F is the Faraday's constant. Due to the small thickness of the RSOFC it can be assumed that the mass transfer of O^{2-} ions from the cathode to the anode of the RSOFC during discharge is sufficiently fast so the concentration of O^{2-} ions in the RSOFC can be regarded as a constant. Since both the cathodic and anodic reaction occurs on the same electrode, the electrical current on an electrode depends on the electrode potential can be described by the Butler-Volmer equation, which gives the anode current density of anode i_n by[26]:

$$i_n = i_{n,0}\{\exp\left[\frac{2\alpha_a F}{RT}\left(\emptyset_n - E_{eq,n}\right)\right] - \exp\left[-\frac{2(1-\alpha_a)F}{RT}\left(\emptyset_n - E_{eq,n}\right)\right]\} \quad \text{.....(16)}$$

Here $\emptyset_n$ is the solid phase electric potential of the anode, $E_{eq,n}$ is the equilibrium potential of the anode, $i_{n,0}$ is the exchange current density for the anode, and $\alpha_a$is the anodic transfer coefficient for the anode. As we have assumed the concentration of O^{2-} ions in the RSOFC is constant, so depending only on the composition of the gas phase species the exchange current density of the anode can be expressed as follows:

$$i_{n,0} = i_{n,0}^{ref} x_1^{1-\alpha_a} x_2^{\alpha_a} \quad \text{.....(17)}$$

Here $i_{n,0}^{ref}$ is the reference-state (where x_1 = 1 and α_a = 0) exchange current density. As we know that the total voltage of the fuel cell at any point in time to the standard electrode potential, temperature, activity and reaction quotient can be determined by the Nernst equation, we can find out the equilibrium potential of the anode from the following equation:

$$E_{eq,n} = E^{\theta}_{eq,n} + \frac{RT}{2F}\ln(^{x_2}/_{x_1}) \quad (18)$$

Here $E^{\theta}_{eq,n}$ is the equilibrium potential at the standard state. The solid phase materials of electrodes usually have large electrical conductivities, so the solid phase electric potential of anode,$\emptyset_n$, can be presented as a function that depends on time only and can be solved by the applied current according to Meng's formulism [26]

$$\frac{1}{A_{\partial\Omega_E}} \iint_{\partial\Omega_E} i_n dS = -i_{app} \quad (19)$$

Here i_{app} is the applied current density on the RSOFC, $\partial\Omega_E$ is the symbol of the RSOFC boundary. $A_{\partial\Omega_E}$ is the area of the ROSFC boundary. i_{app} is defined as positive for charging and negative for discharging. Similar to the anode, the cathode current density is also governed by the Butler-Volmer equation:

$$i_p = i_{p,0}\{\exp\left[\frac{2\beta_a F}{RT}\left(\emptyset_P - E_{eq,p}\right)\right] - \exp\left[-\frac{2(1-\beta_a)F}{RT}\left(\emptyset_P - E_{eq,p}\right)\right]\} \quad (20)$$

Here i_p is the cathode current density and β_a is the anodic transfer coefficient for the cathode, and other symbols have the same physical meanings as in equation for the anode current density. Now for the cathode portion, the condition can be written as:

$$\frac{1}{A_{\partial\Omega_E}} \iint_{\partial\Omega_E} i_p dS = -i_{app} \quad (21)$$

Since we have assumed the cathode of the RSOFC works under constant concentration of O^{2-} ions that means that the partial pressure of oxygen is also constant. So the exchange current density $i_{p,0}$ and equilibrium potential which depends on the partial pressure of oxygen is also constant. From the Butler-Volmer equation of cathode, when a constant

current is applied on a battery $\emptyset_P$ is obtained as a constant form. Now the voltage of the battery E can be found from the difference between the cathode and anode potentials.

$$E = \emptyset_P - \emptyset_n \quad \text{.....(22)}$$

Now the full cell Nernst potential U can be found from the following equation:

$$U = E_{eq,P} - E_{eq,n} \quad \text{.....(23)}$$

and the overvoltage of the battery η is given by:

$$\eta = E - U \quad \text{.....(24)}$$

Chapter 3: Model Configuration

3.1 Constructing the model

The whole mathematical model was developed for this novel battery using COMSOL 4.3 multi-physics software. The whole system is regarded as isothermal so thermal diffusion and heat transfer of the gaseous species are neglected. The transport phenomena of the whole system developed on convective mass transfer of concentrated species. To develop an efficient and computational inexpensive model the whole system developed in a simple one dimensional model. According to the figure 3.1 the whole model is divided into three individual points, in which the first point stands for the RSOFC unit which acts as a variable electrode.

The second point is 1mm apart from the first point, representing the surface of ESU and the third point is 6.3mm apart from the second point, representing the bottom of ESU. The space between the first point and the second point represents the free space for H2-H2O and the space between second point and third point represents the RCU bulk volume (redox cycle unit).

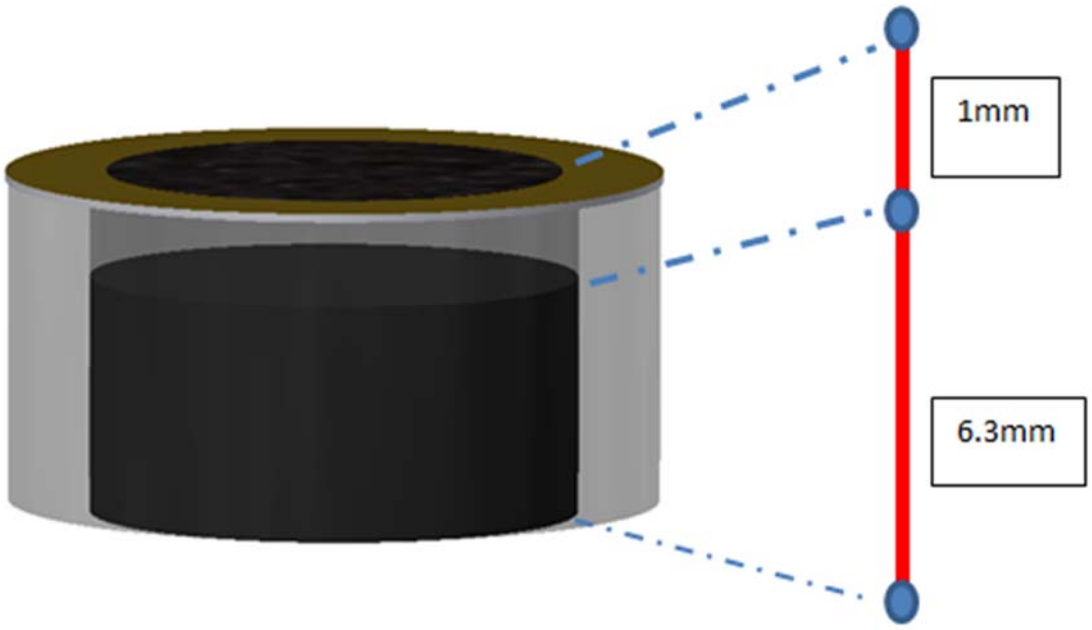

Figure 3.1 : One dimension model

3.2 Computational domain and model settings

The whole system is a time dependent problem which was developed based on physics related transport of concentrated species. In COMSOL the time dependent problem, solved by the direct MUMPS solver with 1.2 memory allocation factor. The mesh settings of that problem determined by the physics controlled mesh and the element size kept extremely fine for an accurate result. The mass transfer of the battery along the whole domain was described by the Maxwell Stefan diffusion equation. As mentioned earlier the first point of

the domain was considered as a variable electrode, a relation can be developed between Maxwell Stefan diffusion equation and electrochemical current density by diffusivity mass flux *(J)*. To solve the reaction rate as a time dependent problem a PDE solver was added to the model, while to solve for the Butler-Volmer equation an ODE solver was added to the model. As mentioned earlier the RCU area is from point two to point three and the H_2-H_2O looping is considered from point one to point two according to figure 3.1. So to distinguish among them, three different sub models were defined. Since it is a time dependent problem to develop a charge discharge profile, an analytic function was added with a reversal current direction being considered from discharge to charge.

3.3 Computational conditions

To conduct the simulation some prerequisite conditions were followed. At the beginning of the discharge the redox metal was considered totally reduced and it was considered totally oxidized at the beginning of the charge cycle. The temperature of the redox material was considered at 800°C. The average current density to conduct simulation was considered at 200mA/cm^2 and the quantity of redox metal in the RCU was considered to be 0.8g. The rates of redox reaction for the forward and the reverse reaction were taken as, respectively, 20s^{-1} and 0.1s^{-1}. The area of the SOFC was 88mm^2 and the density of FeO and Fe were 5500kg/m^3 and 7800kg/m^3, respectively. The parameter values for this model are listed in Table 3.1.

Table 3.1 : Parameters used for the simulations.

Parameter	Value	Unit
$\mathbf{D_{1,2}}$	7.6×10^{-4}	m^2/s
$E_{eq,n}^{\theta}$	-0.941	V
$E_{eq,p}$	0	V
F	96487	C/mol
$i_{n,0}^{ref}$	4.623×10^3	A/m^2
k	20	1/s
$\mathbf{k^{-1}}$	0.1	1/s
P_{ref}	1	atm
R	8.3143	J/mol/K
T	800	°C
V_R	5.63×10^{-6}	m^3
α_a	0.5	
β_a	0.5	
ρ_{Fe}	7.8×10^3	kg/m^3
ρ_{FeO}	5.5×10^3	kg/m^3
$\epsilon_{p,0}$	0.7	

Chapter 4: Modeling Results of SOMARB

The RSOFCs used in the experiment were Electrolyte Supported Button cell purchased from NextCell (Fuel cell materials, Ohio, USA). Table 4.1 lists the compositions of RSOFC. To predict a battery performance under different conditions it is essential to perform simulations of the battery. The numerical results from these simulations are used to facilitate the development of the SOMARB. In the experiment the initial Fe loading for RCU was 0.8g where the initial porosity was 0.7. To get the actual scenario from the simulation the same set of parameters has been used. The operating temperature for the system is fixed at 800℃. The initial mass fractions are $\omega_1 = 0.999$ and $\omega_2 = 0.001$ for H_2 and H_2O, respectively.

Table 4.1 : Compositions and dimensions of the commercial

NextCell[15]		
Component (µm)	**Composition**	**Thickness**
Fuel electrode	**Ni-YSZ/Ni-GDC (interlayer)**	**50**
Electrolyte	**Hionic ZrO2-based**	**150(+/-15)**
Air electrode	**LSM/LSM-GDC(interlayer)**	**50**

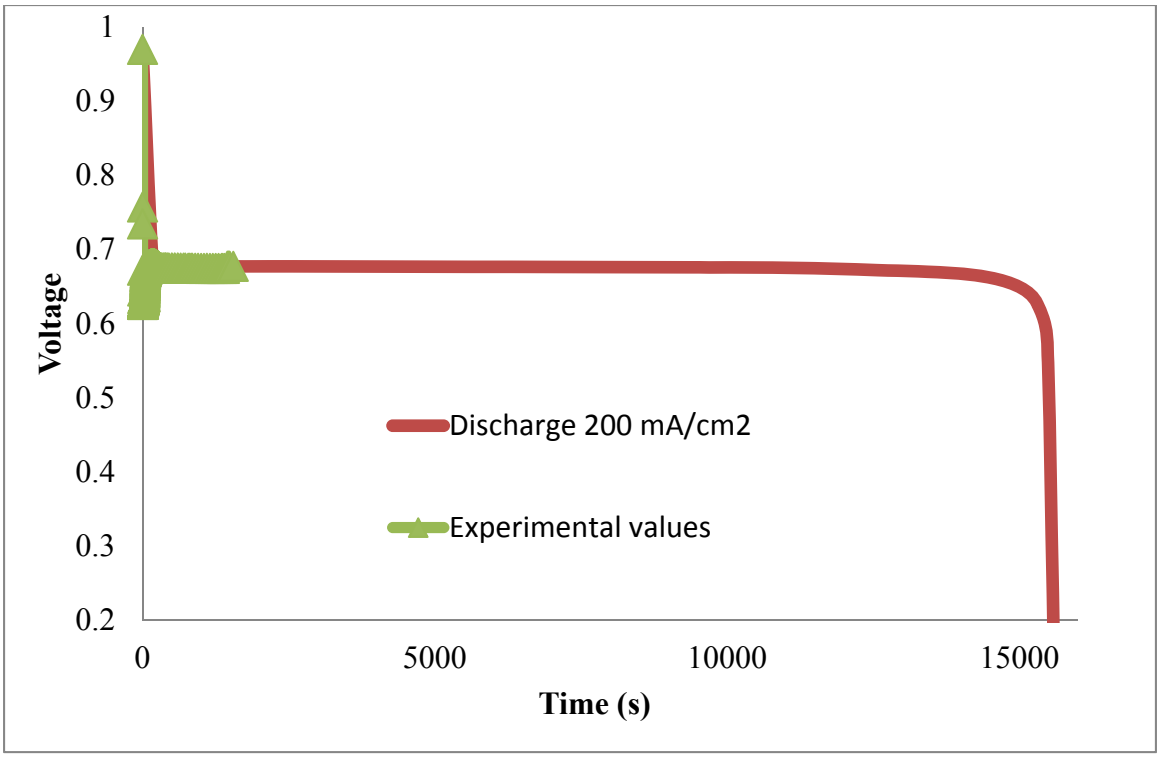

Figure 4.1 : Discharge profile for 200mA/cm^2

4.1 Electrochemical characteristics

To simulate and validate the characteristics of this battery an initial loading 200mA/cm^2 has been considered for discharge and charging. Figure 4.1 shows the simulated results vs experimental voltage profiles under 200mA/cm^2 discharge where SOMARB can discharge for 15500 seconds at 80% depth of discharge (DOD). Experimentally, it is difficult to go for the deep discharge cycle due to limits in its cycle efficiency.

Therefore, only a charge-discharge cycle was performed in around 1020s each for 100 cycles and the voltage trend form the experimental results directly match with the simulation results. From the simulation result, the voltage drops very linearly until 15000s and after that it drops very sharply to its cut off voltage due to the depletion of Fe.

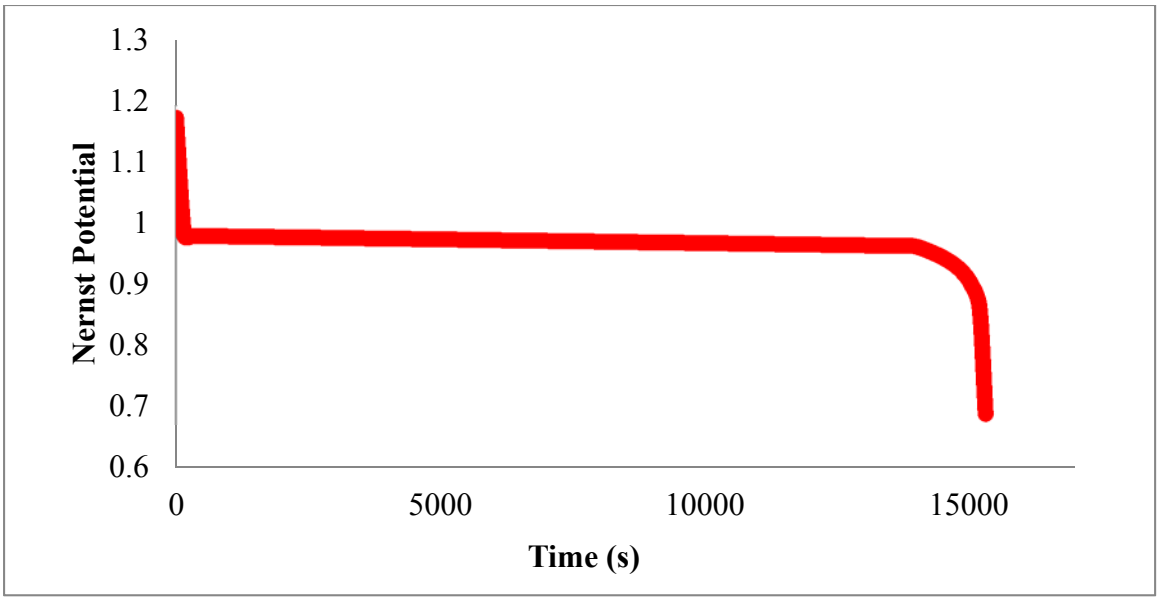

Figure 4.2 : Nernst potential profile under 200mA/cm2

The voltage of the battery remains very linear, because the Nernst potential of the battery is also linear and drops very sharply. From the Nernst equation, the full cell Nernst potential, which is a logarithm function of partial pressures of H_2O and H_2, drops very quickly at the beginning of the discharge because the mole fraction of H_2O is close to zero at that time. According to the electrochemical equation the overvoltage of a battery can be easily defined by subtracting the voltage of a battery from the Nernst potential; the results are shown in Figure 4.2.

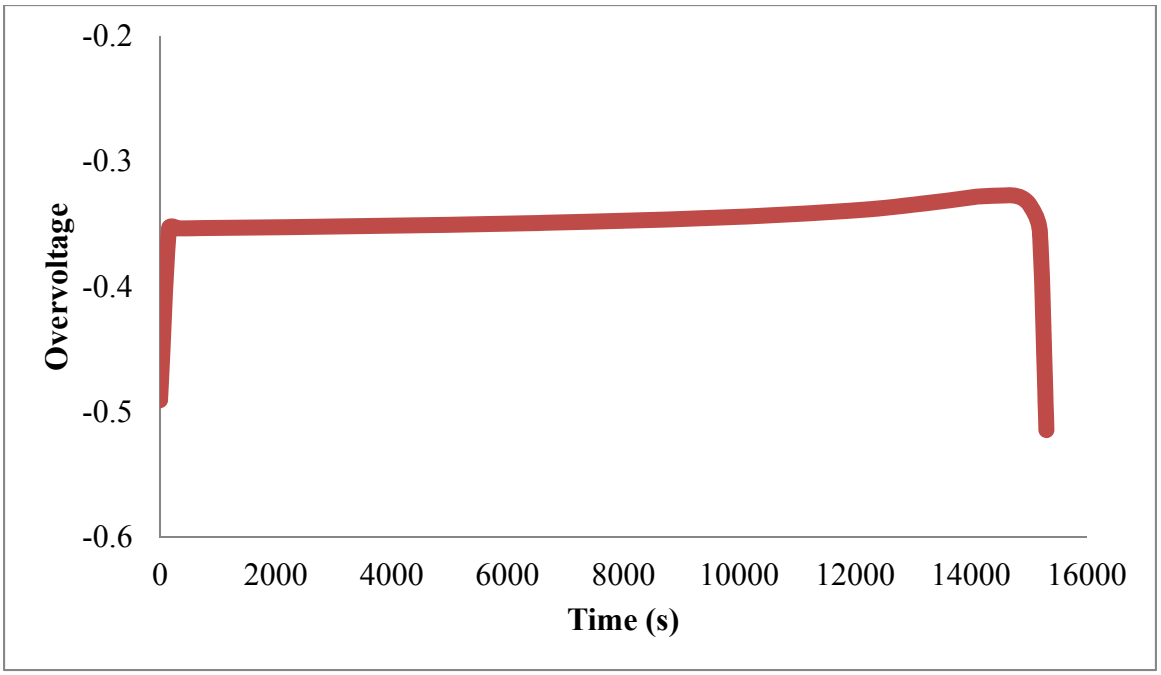

Figure 4.3 : Overvoltage profile of the battery for 200mA/cm^2

According to the Butler-Volmer equation, which is an inverse hyperbolic function of applied current density, the overvoltage decreases very sharply as the discharge begins and counterbalances the drop in Nernst potential. As an outcome the voltage of the battery changes only slightly at the beginning stage of the discharge. From the beginning to the end of this discharge the over-voltage of the battery drops by 0.51V to 0.32V. It is obvious that the discharge profiles change significantly at different applied current densities. Figure 4.4 represents the simulated results vs experimental voltage profiles under 50mA/cm^2 discharge where SOMARB can be discharged for 62719 second at 80% depth of discharge (DOD). Experimentally, however, it is difficult to perform deep discharge due to the concerns on cycle efficiency; only a charge-discharge cycle was performed for 9900s each for 100 cycles. It is apparent that the voltage trend form the experimental results agree well with the simulation results. Since the applied current is small, it would be possible to run for a longer cycle than 200mA/cm^2.

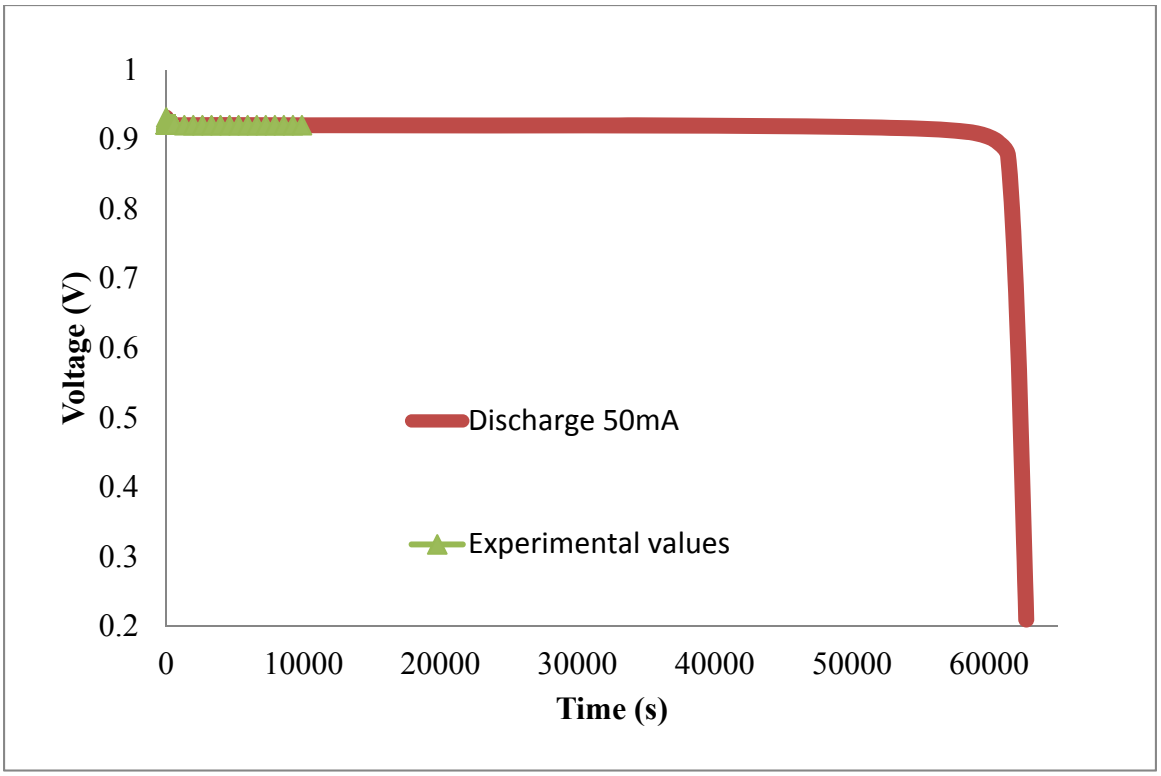

Figure 4.4 : Discharge profile for 50mA/cm^2

4.2 The mass transfer result

At the beginning of the discharge the amount hydrogen is much higher than the amount of steam and when the discharge begins hydrogen reacts with Fe and the Fe-to-FeO conversion makes steam in the system. Figure 4.5 represents the mass fraction of hydrogen and steam for 200mA/cm^2 applied current. Here mass fraction of hydrogen represents 99% at the beginning of the discharge and goes down to near 0.1% when all the Fe of the RCU turns to FeO. On the other hand, the amount of steam is close to 0.1% at the beginning of the discharge and goes up to 99.99% at 80% depth of discharge. Since at the beginning there is no steam in the system, there is a sharp fall of hydrogen mole fraction as well as a sharp rise of steam at the beginning of the reaction. In this battery the hydrogen generating

RCU is located only 1mm apart from the hydrogen consuming RSOFC and also at high temperature the gas phase diffusivity is large (7.6×10^{-4} m^2/s); therefore the mass transfer between the RCU and the RSOFC is sufficiently fast and the system mass balance is limited by the reactions except for the initial stage where concentration gradients in gas phase are not fully developed.

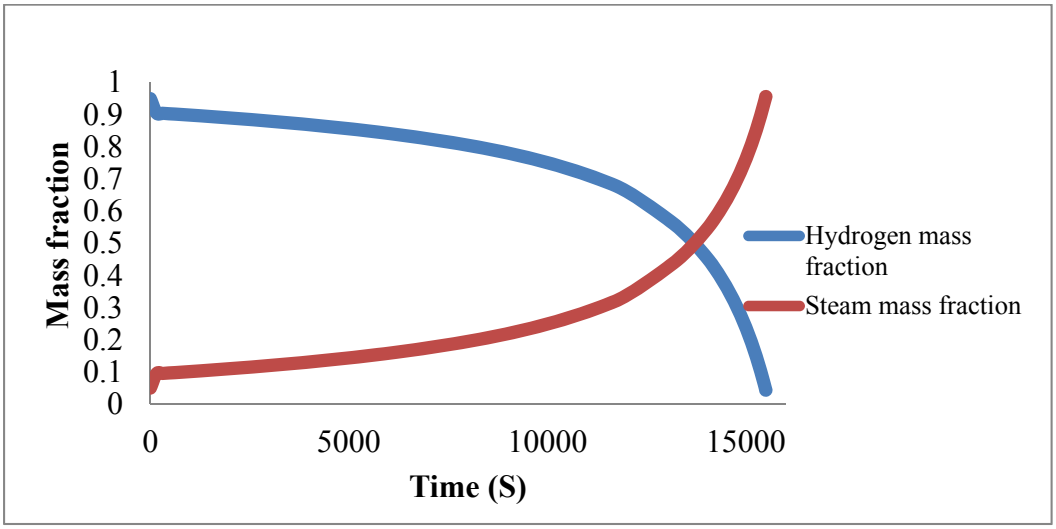

Figure 4.5 : hydrogen and steam mass fraction over time

Figure 4 .6 shows the amount of Fe and FeO where at the beginning of the reaction the full RCU remains Fe and with time it reacts with steam and turns to FeO; thus the amount of FeO increases with time while the amount of Fe decreases. In terms of the material structure of RCU, size of molar Fe is relatively small compared to FeO. Therefore at the beginning when the full RCU is all Fe it is more porous compared to later on. According to the result, the initial porosity of Fe of 0.7 was decreased to 0.54 at the end of discharge.

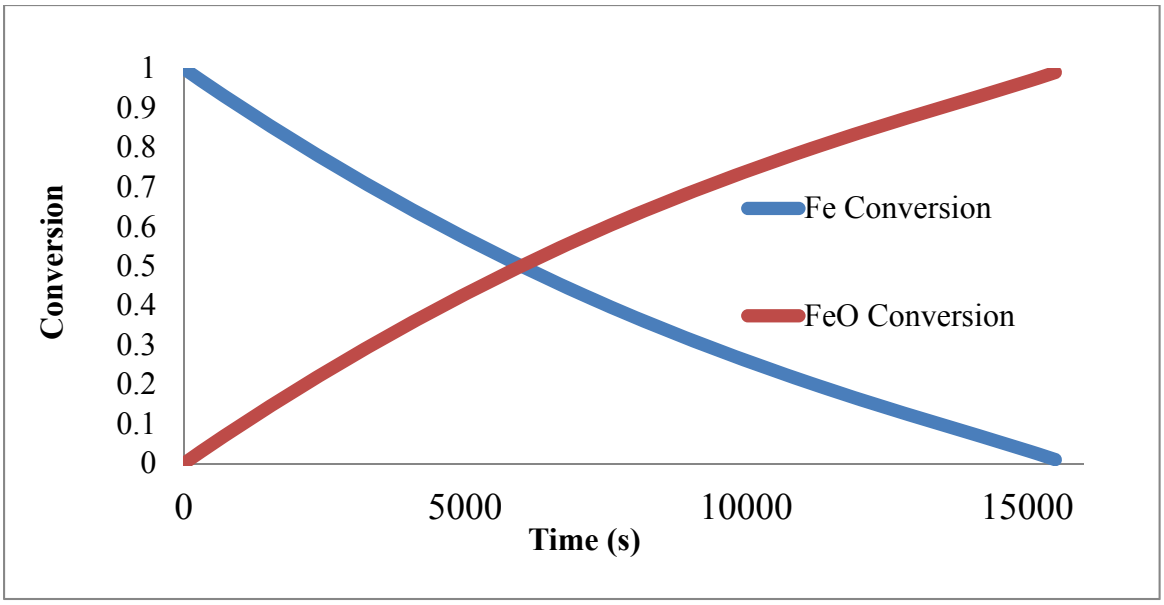

Figure 4.6 : Fe and FeO conversion over time for 200mA/cm^2

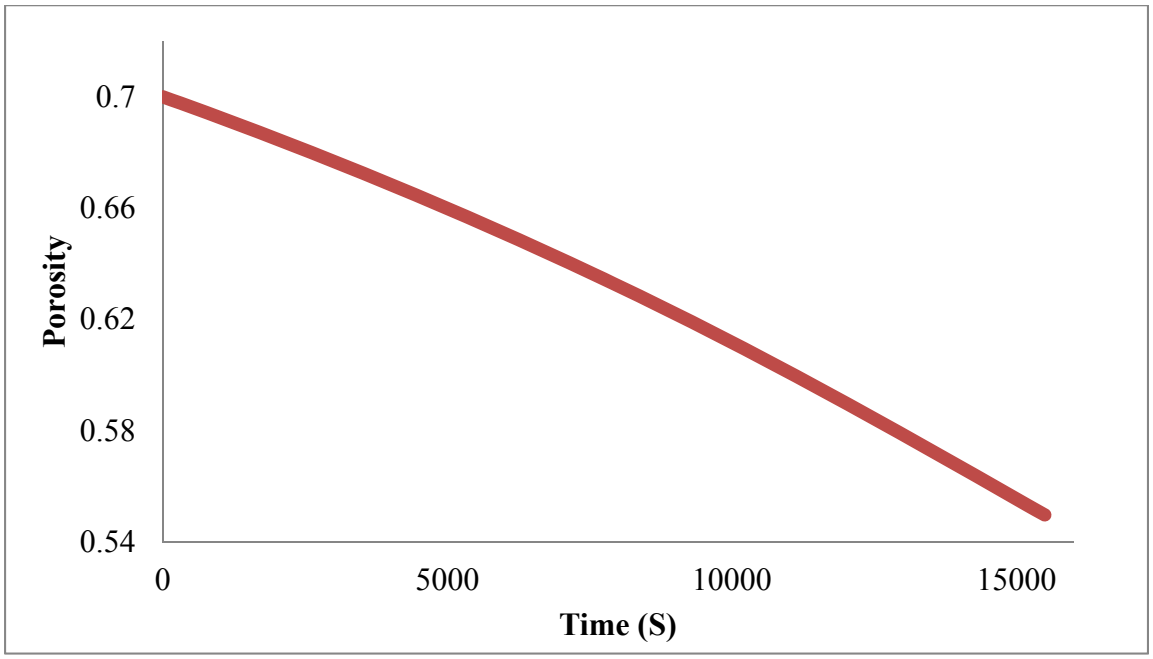

Figure 4.7 : Porosity over time for 200mA/cm^2

4.3 Different current densities effect:

Various discharge profiles are compared at 50, 100 and 200 mA/cm^2 in Figure 4.8. Here the voltage is decreased by 0.25 V when the applied current density is changed from 50mA/cm^2 to 200mA/cm^2. The theoretical capacity of the battery is limited by the loading of Fe material. Figure 4.9 shows the voltage vs capacity profiles for different applied current densities of 50, 100 and 200mA/cm^2. Due to the high ohmic and activation losses at a high current density the cell voltage is generally low. When the current density is increased, the steam generation rate increasing as well as the hydrogen consumption rate also increased which enhances the hydrogen generation rate at RCU. When the hydrogen generation and consumption rate is balanced, a steady state is established and the power generation rate continues until a full amount of Fe is converted to FeO. For different applied current density, the capacity of the battery remains the same as 1086 mAh/g of Fe. The main theme of the battery is that, it consumes the whole amount of Fe from RCU to gain that capacity at different applied current densities. From Figure 4.10 it is shown that almost all the Fe in the RCU has been consumed at the end at each current density.

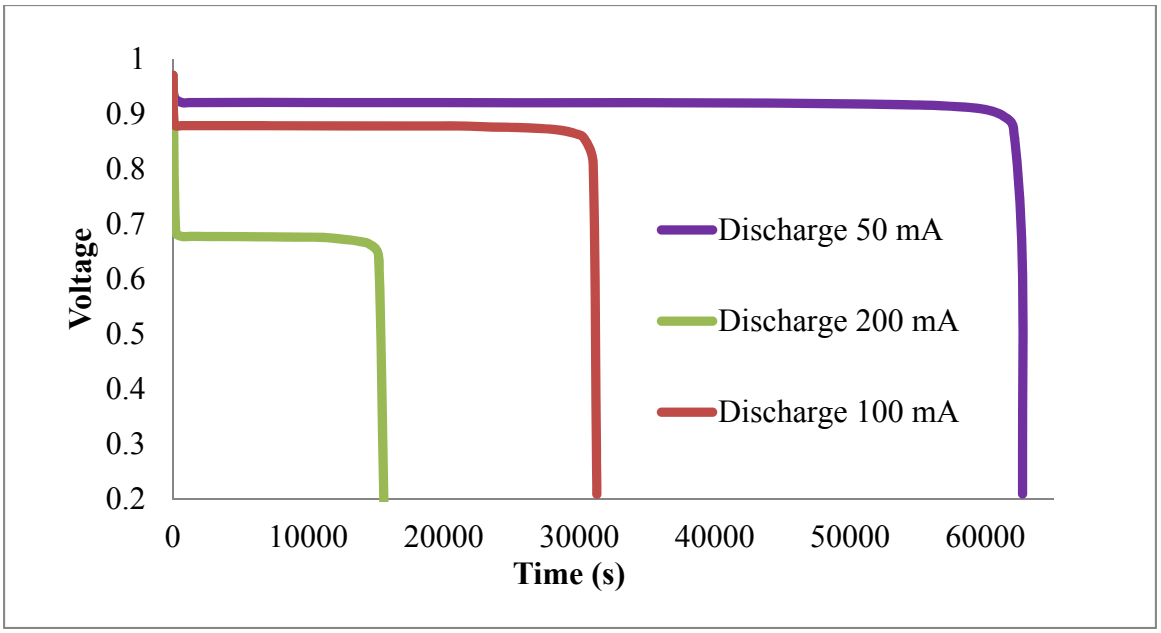

Figure 4.8 : Discharge profile for different applied current densities

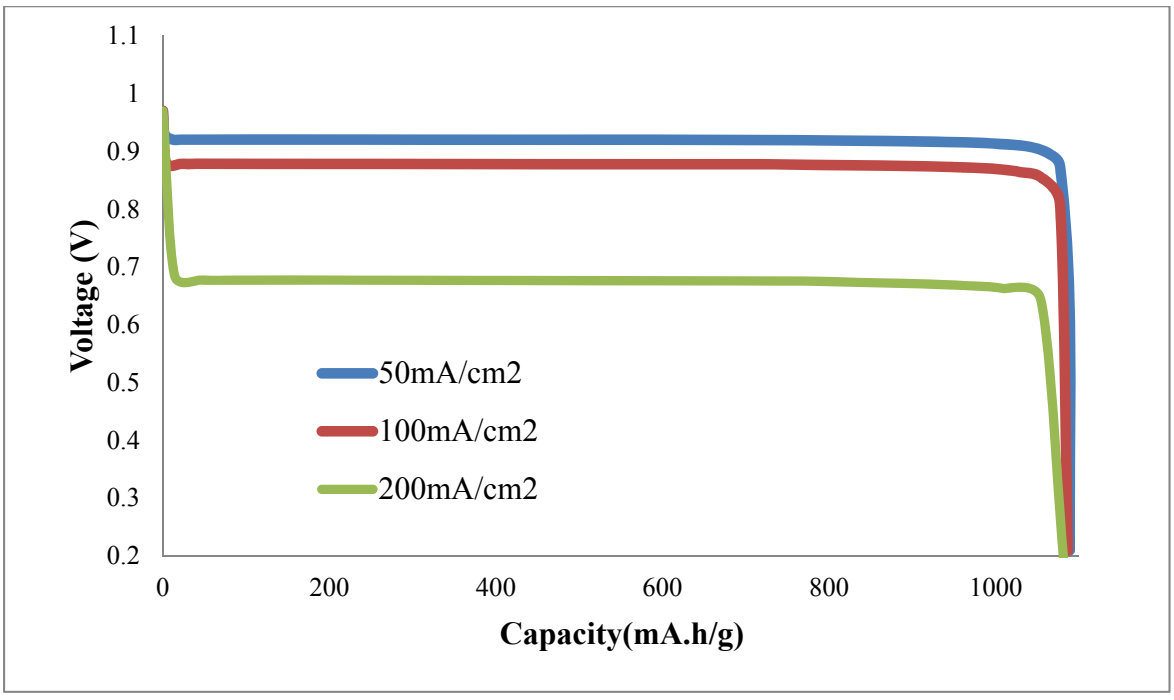

Figure 4.9 : Capacity profile for different applied current densities

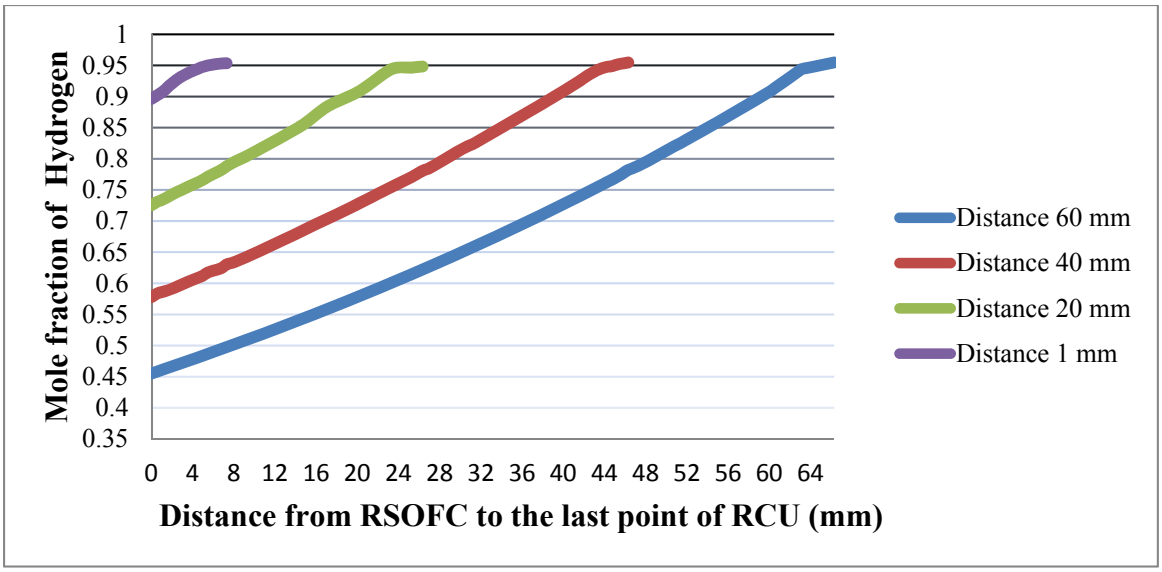

Figure 4.10 : Hydrogen profile for different RSOFC-RCU distances

4.4 Effects of distance between RSOFC and RCU

Typically in the experiment to ensure a higher mass transfer rate the RCU is located close to the hydrogen consuming RSOFC which is around 1mm apart. During discharge cycle the metal is oxidized and generates hydrogen which diffuses to SOFC while hydrogen diffuses in the opposite direction under charge operation. Since metal generates hydrogen, the mole fraction of hydrogen remains higher at RCU and relatively less towards RSOFC. If the distance between RSOFC and RCU is increased the amount of hydrogen towards RSOFC will be decreased. Figure 4.10 shows hydrogen distribution from RSOFC to the end of RCU for different RSOFC-RCU distances. In the simulation the distance from RSOFC to RCU is kept respectively from 1mm, 20mm, 40mm and 60mm. In the figure, it only shows the highest trend of hydrogen distribution from RSOFC to RCU. This hydrogen distribution directly affects the initial drop off voltage of any given applied current density. A greater distance between the RCU and RSOFC would imply lower hydrogen towards

RSOFC which also imply a lower mass transfer flux; this would affect the plateaus of the discharge curve. Figure 4.11 shows the voltage profile of 200mA/cm^2 by keeping the RCU and RSOFC distances 1, 20, 40 and 60mm apart. Here the voltage drops are around 0.03V just by increasing the distance from RCU to RSOFC by 79mm.

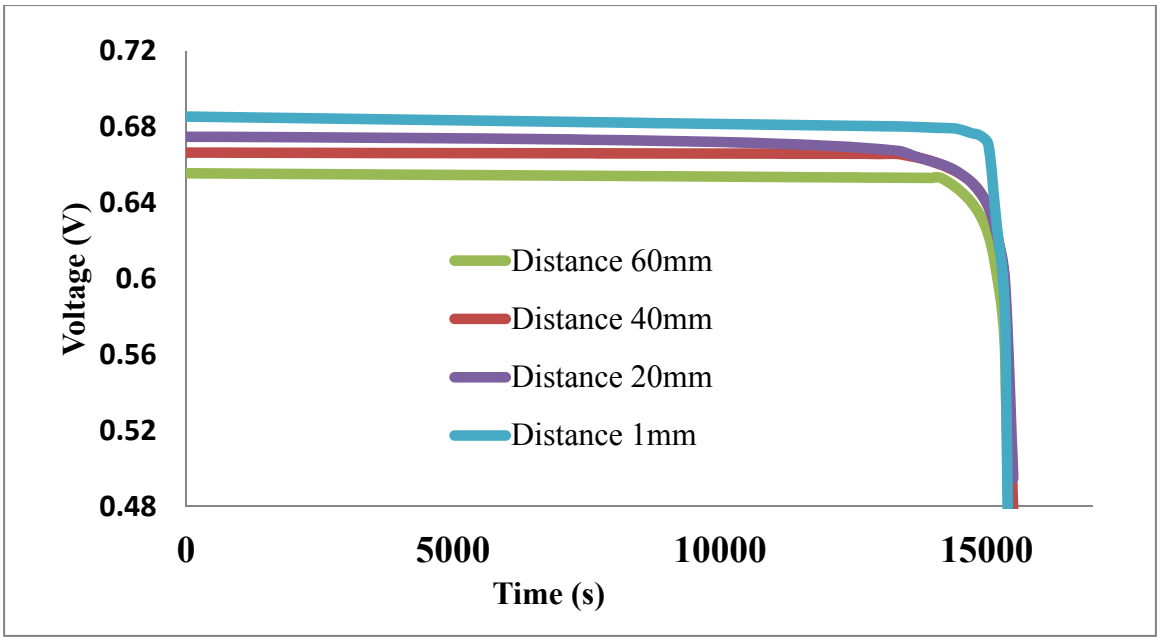

Figure 4.11 : Discharge profiles for different free space variation.

4.5 Charge-Discharge Profile

As previously discussed during the discharge, Fe turns to FeO due to H_2-H_2O looping, in the same way during charging FeO turns to Fe. The molecular size of Fe is smaller than the FeO, so when charge cycle starts right after the discharge cycle the porosity of RCU does not remain same. From figure 4.12, it shows the charging cycle right after the discharge cycle. At the beginning of the discharge when the OCV of the battery was 0.970 volt, the RCU was fully packed with Fe and after 14800s of the discharge when the OCV dropped to 0.38V, the amount of Fe in the RCU became 0.06. After 13200s charging when

the voltage of the battery reached 1.77V, due to the reverse reaction, the amount of Fe at RCU was increased to 0.87.

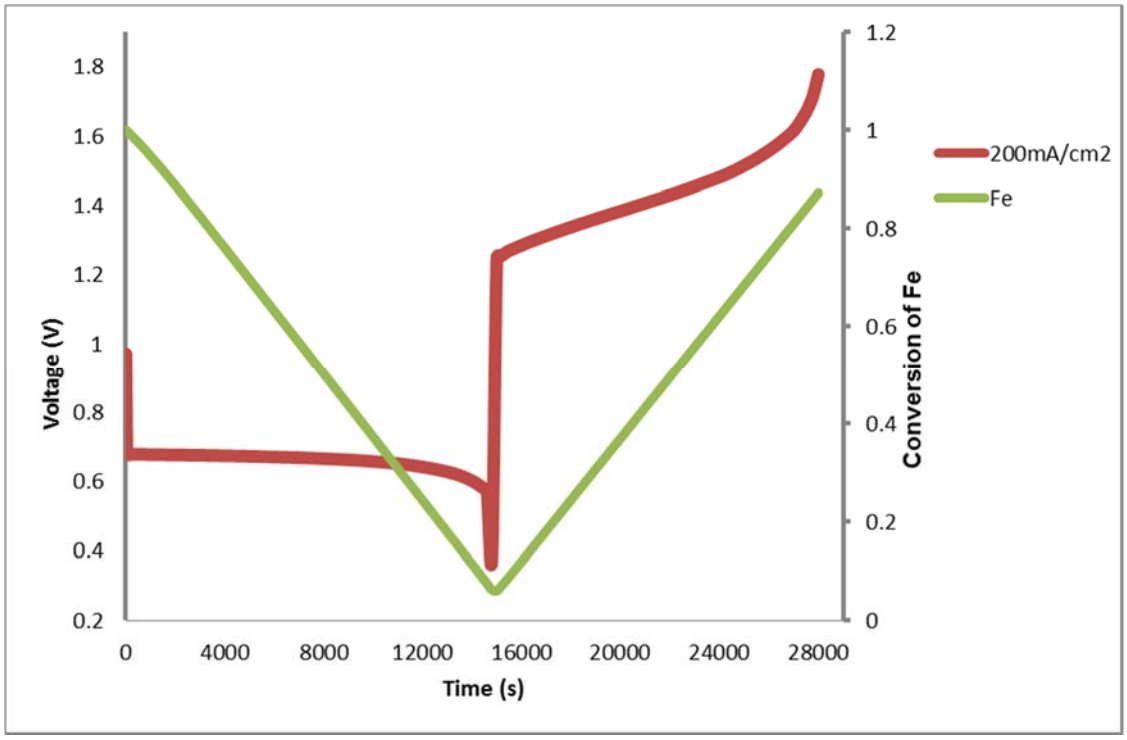

Figure 4.12 : Full charge and discharge profile and volume-average Fe conversion of the battery

At the beginning of the discharge the RCU was packed with Fe and according to figure 4.12 the porosity of RCU was 0.7. During discharge Fe was converted to FeO, so after 14800s of discharge the porosity of RCU descended to 0.55. FeO was converted to Fe during charge cycle so that the porosity of RCU recovered and became 0.68 after 28000s. Again at the beginning of the discharge when the RCU was packed with Fe, the free space between the RCU and RSOFC was packed with hydrogen. According to figure 4.13 when the discharge progressed, the amount of hydrogen mole fraction was decreased while the amount of steam mole fraction was increased. After 14800s of discharge the hydrogen mole

fraction was decreased to 0.31 and at the same time the steam mole fraction was increased to 0.68. After a total cycle of discharge and charge the mole fraction of steam returned to 0.01 where the mole fraction of hydrogen resumed to 0.98.

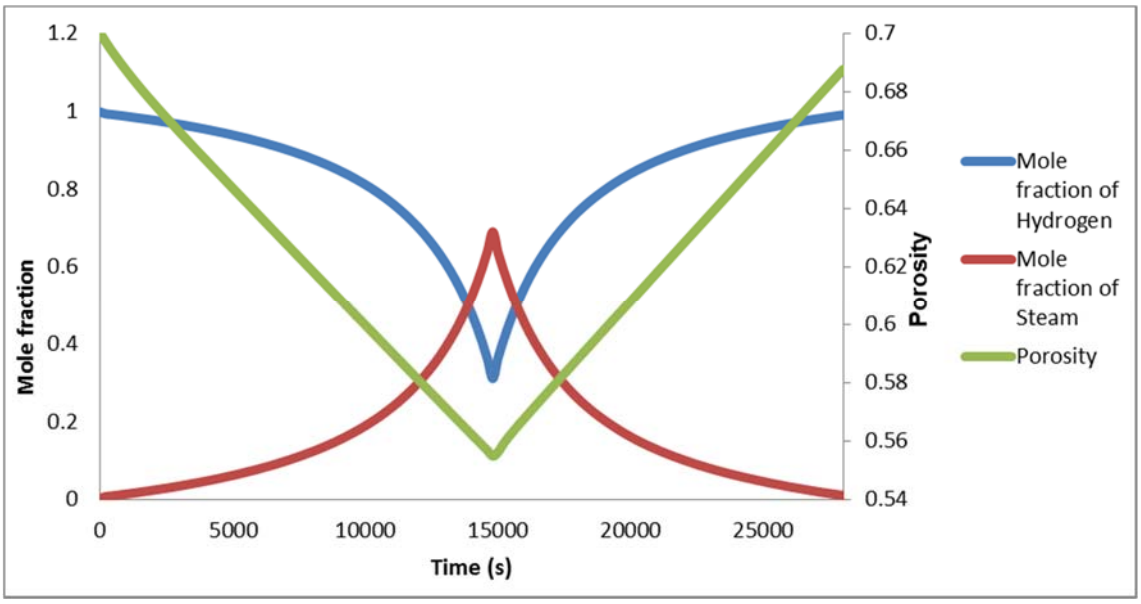

Figure 4.13 : Mole fraction of full charge and discharge profile and volume-average Fe conversion of the battery

4.6 Summary

The modeling results can be summarized as follows:

- With a multiphysics model the fundamental charge/discharge behavior of a solid oxide redox flow battery is numerically predicted.
- The terminal voltage of a solid oxide redox flow battery depends on the mass transfer from RSOFC to RCU and the applied current density.
- The metal redox reaction as well as the electrochemical reaction is an important factor for such kind of redox flow battery. When the balanced reaction proceeds the terminal voltage remains almost constant.
- The distance between the RSOFC and RCU affect the terminal voltage of the battery.
- Temperature plays a very effective role in the mass transfer.

Chapter 5: Concluding Remarks

To build efficient and reliable grid, cost-effective and large scale energy storage systems are the enabling technology, where Rechargeable batteries have great potential to play a critical role. To be the lead in future large scale EES systems, potential rechargeable batteries should have higher energy density, faster response, better efficiency and more diverse design. This masters project investigates and develops physics based mathematical models of a novel rechargeable solid oxide metal-air redox battery (SOMARB) which combines a reversible solid oxide fuel cell (RSOFC) and hydrogen-steam chemical looping component. The energy storage unit (ESU) is physically separated from RSOFC, which keep intact the mechanical integrity of the entire battery structure by allowing it to freely expand and contract. Other novel features which made it distinguished from conventional storage batteries include state-of-charge independent EMF, O^2--enabled high rate and high capacity storage, independent design of power and energy, scalability, sustainability and safety.

To understand the fundamental characteristics of the battery a physics-based mathematical modeling was conducted. The model demonstrates the fundamental electrochemical and the mass transfer characteristics of the battery. To conduct an experiment efficiently, a physics based mathematical modeling is the best way to provide theoretical guidance for the experiments. Various comparative studies including effective

RSOFC-RCU distance, different current densities effect, capacity profile under different applied current densities, volume average Fe conversion effect based on a full charge discharge profile and mole fraction of hydrogen and steam with porosity in RCU etc. have been solved to validate the experimental result as well as to provide good directions for the further research.

One of the main characteristics of such kind of battery is the balance reaction rate. At a certain applied current density when the hydrogen generation and consumption rate is balanced, a steady state is established and this phenomenon came out perfectly from this simulation. The Nernst potential profile and the overvoltage profile of this battery showed the true effect of this phenomenon. Voltage profile depends on the applied current density. Due to the high ohmic and activation losses, at a high current density the cell voltage remains generally low and from the simulation at different current densities, the voltage profile and the capacity profile proved this features. Voltage profile also depends on the distance between RSOFC and RCU. Since metal-steam reaction generates hydrogen, the mole fraction of hydrogen remains higher at RCU and relatively less towards RSOFC. If the distance between RSOFC and RCU is increased the amount of hydrogen towards RSOFC will be decreased. This hydrogen distribution directly affects the initial drop off in voltage at any given applied current density. A greater distance between the RCU and RSOFC would imply lower hydrogen concentration towards RSOFC which also imply a lower mass transfer flux; this would affect the plateaus of the discharge curve. A full charge-discharge cycle reflects the real aspect of a rechargeable battery. Fe turns to FeO due to H_2-H_2O looping during discharge and in the same way during charging FeO turns to Fe. At the beginning when the full RCU is packed with Fe, it remains more porous

compared to later period. So during discharge when Fe turned to FeO, porosity of RCU is reduced and in the same way during charge cycle when FeO turned to Fe the porosity is increased. Molar fraction of hydrogen is reduced during the discharge cycle and is gained during the charge cycle. Molar fraction of steam reacts in the same way like the hydrogen mole fraction. All the simulated voltage profile under different current densities agreed well with the experimental results.

Chapter 6: Future Work

A lot of improvements can be made in this simulation work in future.

- Two dimensional or a three dimensional simulation should be conducted.
- Temperature effect on the battery characteristics should also be investigated. For iron-based system, the redox couple varies with temperature. This simulation solved under a constant temperature of 800℃ so further comparative effects on temperature effect can be solved. Here for 800℃ the redox reaction with Fe and steam turns to FeO and H_2O. But for 500℃ steam oxidizes Fe and turns to Fe_3O_4, so to develop a further lower temperature simulation, can be conducted by based on this redox reaction

$$4H_2O + 3Fe \underset{charge}{\overset{discharge}{\rightleftharpoons}} 4H_2 + Fe_3O_4$$

- The effect from a different redox couple because of temperature change should also be studied.
- In this simulation the whole system is regarded as isothermal so thermal diffusion and heat transfer of the gaseous species are neglected. By considering heat transfer effect a more rigorous simulation can be solved.

- The degradation of redox material is not considered in this study. In the future, multiple charge-discharge cycles should be simulated with the consideration of degradation mechanisms.

References

1. Wang, J.-G., et al., *Synthesis and electrochemical performance of MnO< sub> 2</sub>/CNTs–embedded carbon nanofibers nanocomposites for supercapacitors.* Electrochimica Acta, 2012. **75**: p. 213-219.
2. Salari, M., K. Konstantinov, and H.K. Liu, *Enhancement of the capacitance in TiO2 nanotubes through controlled introduction of oxygen vacancies.* Journal of Materials Chemistry, 2011. **21**(13): p. 5128-5133.
3. Zhao, P., et al., *Nickel foam and carbon felt applications for sodium polysulfide/bromine redox flow battery electrodes.* Electrochimica Acta, 2005. **51**(6): p. 1091-1098.
4. Cui, Y.F., et al., *Novel Anion Exchange Membranes from Poly (aryl ether) s with Quaternary Guanidinium Groups.* Advanced Materials Research, 2012. **560**: p. 864-868.
5. Yang, Z., et al., *Electrochemical energy storage for green grid.* Chemical Reviews, 2011. **111**(5): p. 3577-3613.
6. Huggins, R.A., *Energy storage*. 2010: Springer.
7. Dustmann, C.-H., *Advances in ZEBRA batteries.* Journal of Power Sources, 2004. **127**(1): p. 85-92.
8. Blurton, K.F. and A.F. Sammells, *Metal/air batteries: Their status and potential—a review.* Journal of Power Sources, 1979. **4**(4): p. 263-279.

9. Nestoridi, M., et al., *The study of aluminium anodes for high power density Al/air batteries with brine electrolytes.* Journal of Power Sources, 2008. **178**(1): p. 445-455.

10. Leskes, M., et al., *Direct Detection of Discharge Products in Lithium–Oxygen Batteries by Solid-State NMR Spectroscopy.* Angewandte Chemie, 2012. **124**(34): p. 8688-8691.

11. Malkhandi, S., et al., *Self-Assembled Monolayers of n-Alkanethiols Suppress Hydrogen Evolution and Increase the Efficiency of Rechargeable Iron Battery Electrodes.* Journal of the American Chemical Society, 2012. **135**(1): p. 347-353.

12. Lu, Y.-C., et al., *In situ ambient pressure X-ray photoelectron spectroscopy studies of lithium-oxygen redox reactions.* Scientific reports, 2012. **2**.

13. McCloskey, B.D., et al., *On the mechanism of nonaqueous Li–O2 electrochemistry on C and its kinetic overpotentials: some implications for Li–air batteries.* The Journal of Physical Chemistry C, 2012. **116**(45): p. 23897-23905.

14. Xu, N., et al., *A novel solid oxide redox flow battery for grid energy storage.* Energy & Environmental Science, 2011. **4**(12): p. 4942-4946.

15. Zhao, X., et al., *Energy storage characteristics of a new rechargeable solid oxide iron–air battery.* RSC Advances, 2012. **2**(27): p. 10163-10166.

16. Zhao, X., et al., *Performance of Solid Oxide Iron-Air Battery Operated at 550° C.* Journal of The Electrochemical Society, 2013. **160**(8): p. A1241-A1247.

17. Zhao, X., et al., *Solid Oxide Iron-Air Rechargeable Battery-A New Energy Storage Mechanism.* ECS Transactions, 2013. **50**(45): p. 115-123.

18. Zhao, X., et al., *Long Term Stability Study of a Solid Oxide Metal-Air Battery.* ECS Transactions, 2013. **45**(29): p. 113-121.

19. Zhao, X., et al., *A high energy density all solid-state tungsten–air battery.* Chemical Communications, 2013. **49**(47): p. 5357-5359.

20. Landes, H. and R. Reichenbacher, *Enhancement of Oxygen Transport in the Storage Electrode of a High Temperature Secondary Metal-Air Battery Based on an Oxygen Ion Conducting Electrolyte.* ECS Transactions, 2013. **50**(25): p. 47-68.

21. Inoishi, A., et al., *Fe–air rechargeable battery using oxide ion conducting electrolyte of Y< sub> 2</sub> O< sub> 3</sub> stabilized ZrO< sub> 2</sub>.* Journal of Power Sources, 2013. **229**: p. 12-15.

22. DANIELS, F., *A TABLE OF QUANTUM YIELDS IN EXPERIMENTAL PHOTOCHEMISTRY1.* The Journal of Physical Chemistry, 1938. **42**(6): p. 713-732.

23. Wagner, C., *Über den Mechanismus der elektrischen Stromleitung im Nernststift.* Naturwissenschaften, 1943. **31**(23): p. 265-268.

24. Doenitz, W. and R. Schmidberger, *Concepts and design for scaling up high temperature water vapour electrolysis.* International Journal of Hydrogen Energy, 1982. **7**(4): p. 321-330.

25. Ohmori, H., S. Uratani, and H. Iwai, *Numerical simulation of gas diffusion effects on charge/discharge characteristics of a solid oxide redox flow battery.* Journal of Power Sources, 2012. **208**: p. 383-390.

26. Guo, M., et al., *A Multi-Physics Model for Solid Oxide Iron-Air Redox Flow Battery: Simulation of Discharge Behavior at High Current Density*. Journal of The Electrochemical Society, 2013. **160**(11): p. A2085-A2092.

27. Multiphysics, C. O. M. S. O. L. "Chemical Engineering Module–User's Guide." COMSOL, COMSOL 3 (2008).